Substitution of Nanocrystalline Toroid by Laminated Ferrite Toroid in the Application of a Common-Mode Choke

Lukas Reißenweber, Fritz Wohlrath, Alexander Stadler
COBURG UNIVERSITY OF APPLIED SCIENCES AND ARTS
Friedrich-Streib-Str. 2
Coburg, Germany
E-Mail: lukas.reissenweber@hs-coburg.de
URL: http://www.coburg-university.de

Keywords

«Ferrite», «Impedance measurement», «EMC/EMI», «Filter optimization», «Filtering», «Nanocrystalline Core»

Abstract

In this work, it is investigated if a nanocrystalline toroid of a common-mode (CM) choke can be substituted by a laminated ferrite toroid. Small-signal measurement results of the complex impedance, of laminated toroidal cores of the material T38 with different diameters and layer thicknesses at 25 °C and 100 °C, are presented. Further, the calculated attenuation and the complex permeability are shown. Based on the obtained material data, a CM choke made of a laminated ferrite core is designed and analyzed. The focus is thereby on the comparison with the nanocrystalline CM choke.

Introduction

The high frequencies enabled by SiC- and GaN-semiconductors increase the efficiency of power electronic circuits and lead to a reduction of the component size of passive components, thus reducing the costs. However, the steep voltage rises also lead to undesirable amplitudes at higher frequencies. To meet electromagnetic compatibility (EMC) requirements, these must be damped if they cannot be avoided. The CM chokes made of ferrites have been more and more replaced since the development of the nanocrystalline cores. Ferrites are classified into MnZn and NiZn type, which is more suitable for high frequencies (higher Q-factor due to lower eddy-currents as a result of lower electrical conductivity). However, NiZn ferrites have a lower permeability ($\mu'_{r,25°C}$: 15 - 2300) and lower saturation flux density ($B_{sat.,25°C}$: 0.22 - 0.42 T) compared to MnZn ferrites ($\mu'_{r,25°C}$: 350 - 20000, $B_{sat.,25°C}$: 0.31 - 0.55 T) [1-3]. The nanocrystalline material is particularly suitable compared to ferrite due to the higher permeability ($\mu'_{r,25°C}$: 100 - 250000) and higher saturation flux density ($B_{sat.,25°C}$: 0.32 - 1.45 T) [4, 5]. Its real part of the permeability decreases above a certain frequency (around kHz) gradually as frequency increases. Compared to that, the ferrite drops abruptly around MHz (s. fig. 10). In addition, nanocrystalline cores have a low temperature dependence [4]. However, it is a more expensive material. A replacement by a less expensive material such as ferrite is therefore desirable. Investigations on laminated ferrite cores have shown that macroscopic eddy-current losses can be reduced and the impedance at higher frequencies can be increased [6-8].

Fundamentals of substitution of a nanocrystalline toroidal core

When designing a CM filter, it must be known what insertion loss or impedance is required. Typically, the spectrum of interference of the circuit is first measured without a filter. Then the permissible interference is subtracted according to the used standard [e.g. EN55011, EN55012, EN55025 or EN55032]. The result is the spectrum to be damped and so the required insertion loss or filter impedance is known [9, 10]. When developing a CM choke, macroscopic eddy-current losses and dimensional effects must be considered. The greater the difference between the inner and outer radius, the more inhomogeneous is the flux distribution over the cross-section. In addition, the size of the cross-sectional area is quadratically affected by the occurring eddy-currents and their corresponding opposing fields

[6, 7, 11-14]. Fig. 1 a) shows the magnitude of the complex impedance normalized to the 10 kHz value and b) the argument of different sized toroidal cores (R16, R25 and R63) of the material T38 at $\vartheta = 25$ °C. It can be seen that due to the reasons mentioned above, the largest core already loses impedance at lower frequencies. Also, the argument of the larger cores first falls to zero and below.

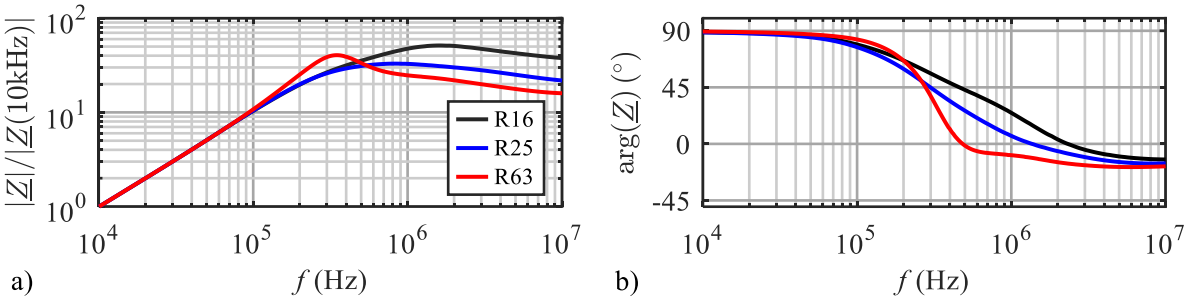

Fig. 1: a) Normalized magnitude, b) argument of different sized toroidal cores made of T38 at 25 °C.

The effect of the opposing fields caused by eddy-currents is illustrated in fig. 3, using a 2D axial symmetric magnetic FEM simulation. It shows the distribution of magnetic field strength H_φ in the core cross-section at different frequencies normalized to the highest occurring field strength $H_{\varphi,max}$. Static values for the real part of the relative permeability $\mu_r' = 1 \cdot 10^4$, the electrical conductivity $\kappa = 6$ S/m and the real part of the relative permittivity $\varepsilon_r' = 1 \cdot 10^5$ are used. Such distributions are experimentally verified by measurements in [6, 7]. The upper row shows the field distribution of a R16 core as frequency increases. At $f = 1$ kHz, the field distribution is almost homogeneous, affected only by the different radii. At $f = 300$ kHz the field reducing effect occurs due to the opposing fields of the eddy currents. At $f = 1$ MHz, these opposing fields are so strong that negative field strength values occur in the center of the core. The effect is even more significant in the larger R63 core. This is clearly shown by the comparison of the field distribution at $f = 300$ kHz. The consequence is a reduction of the inductance (real part of complex permeability) with simultaneously increasing losses. The bottom row shows a laminated R63 core. Due to the smaller cross-sectional areas, the macroscopic eddy-currents are significantly reduced. This is shown by the nearly unchanged flux distribution with increasing frequency between $f = 1$ kHz and $f = 300$ kHz. Such a design of a larger ferrite core can therefore increase the frequency range at which it can be used [6-8]. This is examined here using toroidal cores of the sizes R16, R25 and R63 with different layer thicknesses made of the material T38. A detailed analytical analysis for calculation of core loss and structural effects is provided in [15, 16].

Investigations on laminated T38 toroids

Prototypes

Table I provides an overview of all investigated core samples and their number. $N_{lam.}$x$h_{lam.}$ is the name, where $N_{lam.}$ is the number of layers and $h_{lam.}$ the layers thickness. A selection of cores is shown in fig. 2.

Table I: Overview of the investigated core samples.

Core	$N_{lam.}$x$h_{lam.}$	Nbr. of samples	a [mm]	b [mm]	h [mm]	l_e [mm]	A_e [mm²]	$B_{sat.,25°C}$ [T]	$B_{sat.,100°C}$ [T]
R16	1x4mm	4	4.80	8.00	4.00	38.52	12.53	0.43	0.26
	2x2mm	4							
	4x1mm	4							
R25	1x8mm	3	7.40	12.65	8.00	60.07	41.01		
	2x4mm	3							
	4x2mm	3							
	8x1mm	2							
R63	1x20mm	3	12.50	31.50	20.00	152.09	244.74		
	2x8mm	1			16.00		195.79		
	6x2.5mm	2			15.00		183.56		
Nanocrystalline		2	10.00	15.00	15.00	76.43	51.79 (ff 70%)	1.10	

The layers of the sizes R16 and R25 were produced by milling and subsequent grinding. In order to exclude that the machining process has an influence on the material properties, test samples were additional manufactured using a diamond wire saw. Independent on the varying machining process the same results were obtained. The R63 layers were produced only by diamond wire saw. In order to obtain rectangular cross-sections, the chamfered upper and lower sides of the bulk cores were removed.

Fig. 2: Prototypes of bulk and laminated R16, R25 and R63 toroidal cores made of T38.

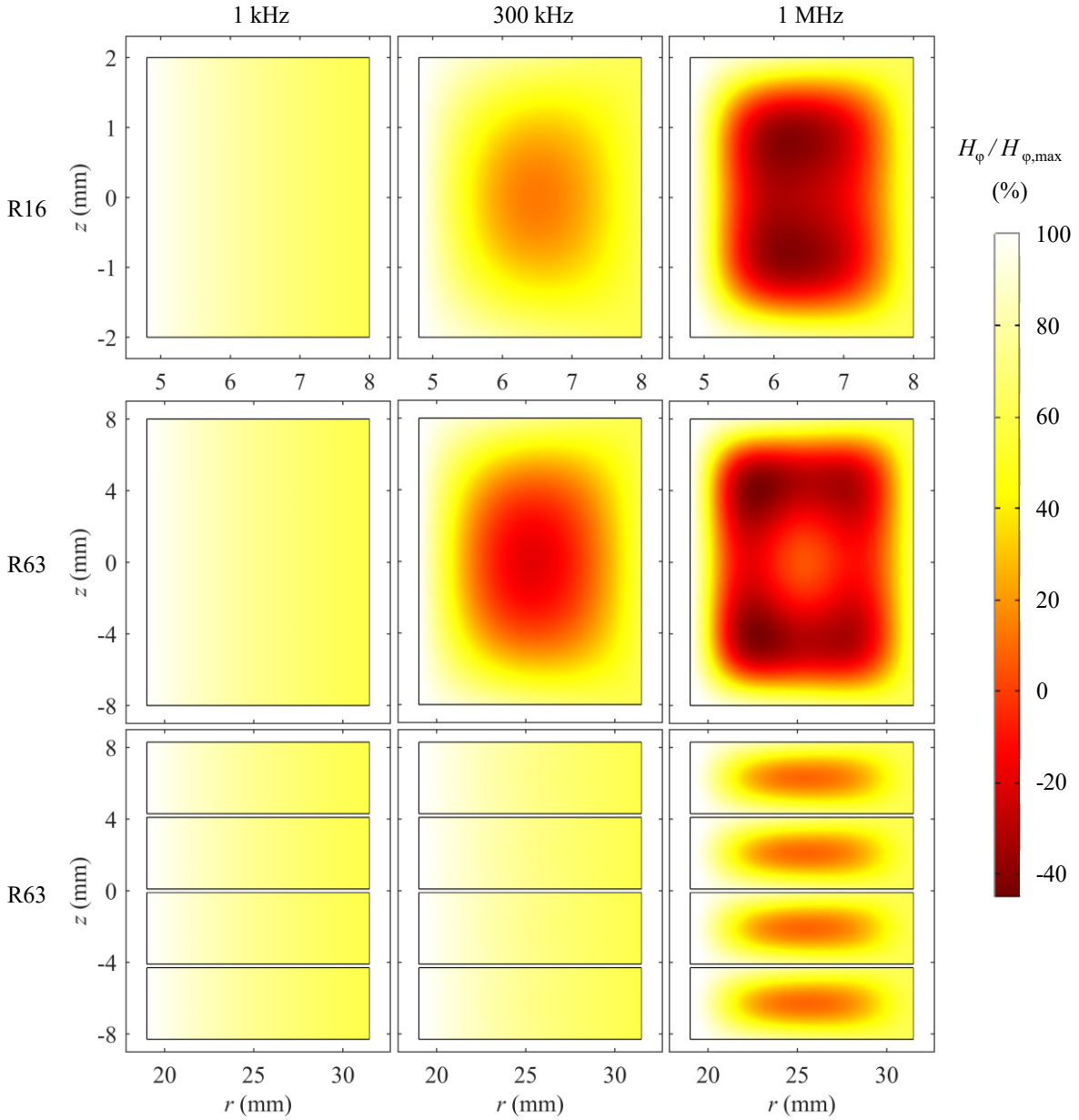

Fig. 3: 2D axial symmetric magnetic FEM simulation of the magnetic field in R16, bulk and laminated R63 toroidal cores at f = 1 kHz, f = 300 kHz and f = 1 MHz.

Adhesive strips serve as spacers. The fact that these have no influence on the measurement results was proven by measurements without them. All measurements were carried out in a coaxial cartridge manufactured for each core size according to the design in [17]. To eliminate the influence of premagnetization, the samples were demagnetized in advance. In the evaluation, the average values from all measurements of the respective size are shown.

Extension of the frequency range of complex permeability by lamination

The complex permeability of ferrites is influenced by a variety of parameters. These include the material composition, the sintering process, the geometry and the size of a core. The curves of complex permeability presented below are based on small-signal measurements. The equations from standard [IEC-60205] are used for the effective length l_e and the effective cross-section A_e:

$$l_e = 2\pi \frac{ab}{b-a} \cdot \ln\frac{b}{a} \tag{1}$$

$$A_e = h \frac{ab}{b-a} \cdot \left[\ln\frac{b}{a}\right]^2 \tag{2}$$

Therein, parameter a denotes the inner and parameter b the outer radius. The height h of the laminated cores is the sum of the number of layers and their height ($N_{lam.}$x$h_{lam.}$). The calculation of the complex permeability is based on the effective core parameters (1, 2), the magnetic field constant μ_0, the square of the number of turns N, the angular frequency ω and the real or imaginary part of the measured complex impedance $\underline{Z}$ [3, 4]:

$$\mu_r' = \frac{\mathrm{Im}\{\underline{Z}\}}{\omega \cdot \mu_0 \cdot N^2 \cdot (A_e/l_e)} \tag{3}$$

$$\mu_r'' = \frac{\mathrm{Re}\{\underline{Z}\}}{\omega \cdot \mu_0 \cdot N^2 \cdot (A_e/l_e)} \tag{4}$$

Fig. 4 a) shows the complex permeability of the core size R25 at $\vartheta = 25$ °C. It can be seen that with decreasing layer thickness the real part of the permeability is more stable up to higher frequencies. Losses also decrease, but extend toward higher frequencies due to the longer lasting real part. Fig. 4 b) depicts the curves at $\vartheta = 100$ °C. Fig. 5 a) shows the real part of the complex permeability of the bulk R16, R25 and R63 cores and their laminated versions with the thinnest layer thickness investigated. In fig. 5 b), the corresponding imaginary part of the cores are shown. Overall, the previously explained behavior is evident here. In the case of the R25 cores, the lamination achieves a behavior that is nearly similar compared to that of the R16 core. In addition, the mechanical machining of the cores always leads to a change in magnetic properties. We assume that this depends on a change in internal mechanical stresses. A decrease in the real part of the permeability of up to -27.7 % for the R16 core and -27.6 % for the R25 core was observed. For R63, an increase of 9.2 % was measured.

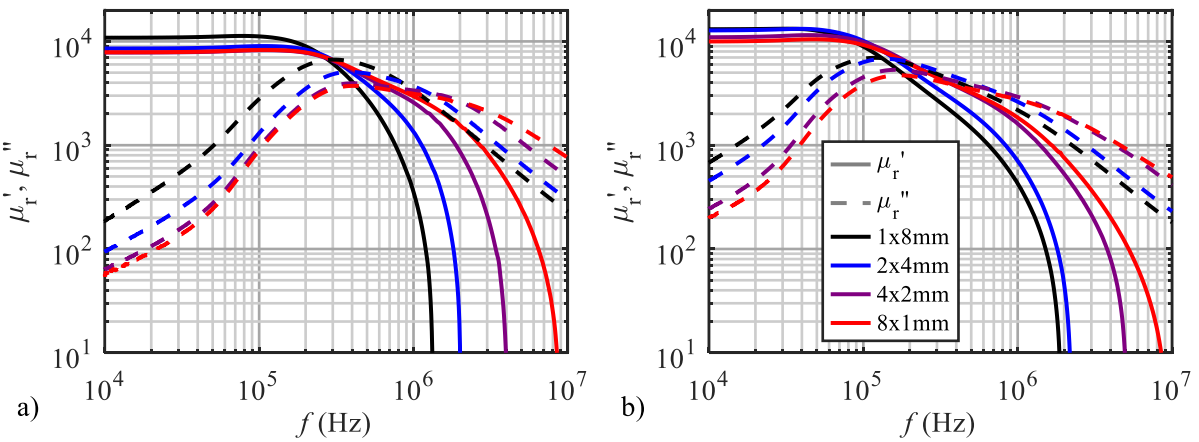

Fig. 4: Complex permeability of bulk and laminated R25 toroids made of T38 at a) $\vartheta = 25$ °C and b) $\vartheta = 100$ °C.

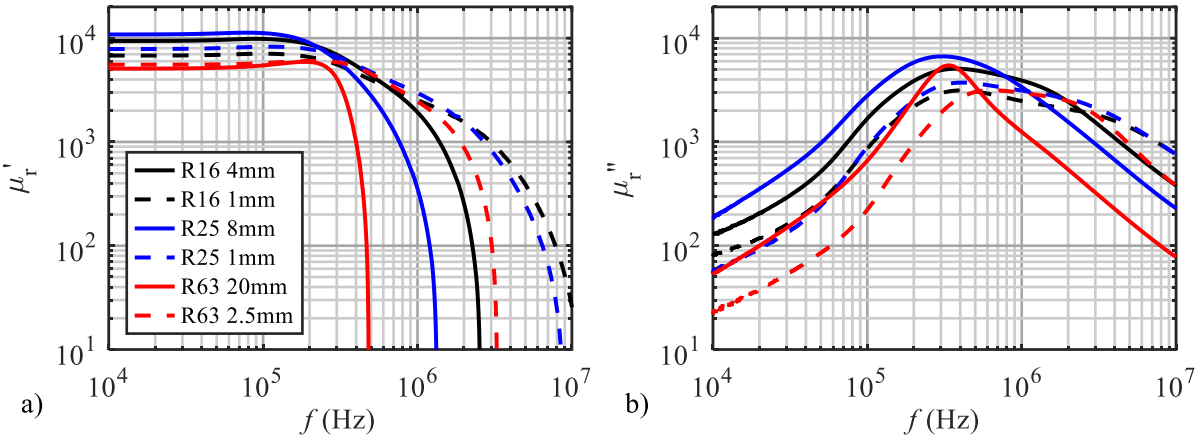

Fig. 5: Complex permeability of bulk and laminated R16, R25 and R63 cores made of T38 at $\vartheta = 25°C$, a) real and b) imaginary part.

Distribution of permeability in axial-direction

When measuring the individual layers of the R63 cores with a layer thickness of $h_{lam.} = 2.5$ mm, a distribution of the real part of the permeability was observed. Fig. 6 shows the averaged values of the two prototypes at $\vartheta = 25$ °C and a frequency of $f = 10$ kHz. It can be seen that, with the exception of the chamfered top and bottom layer, the permeability decreases from S01 to S03 and then increases again from S04 to S06. In this case, the top and bottom layers deviate from the systematic. Such a distribution can already be introduced in the core by the manufacturing process (position of the parting plane of pressing tool). For the exact knowledge of the flux distribution, this has to be considered.

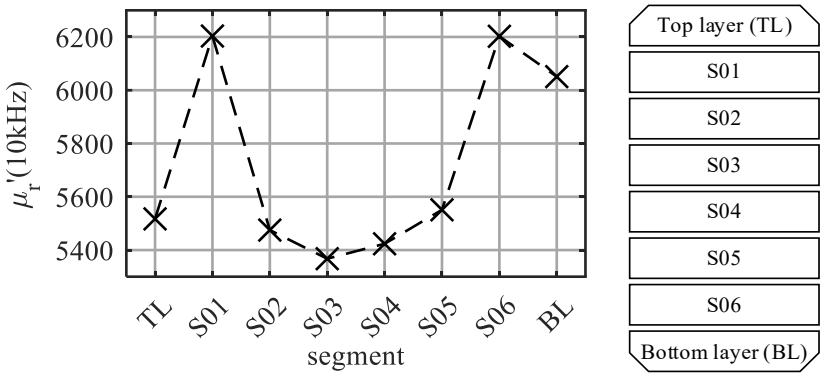

Fig. 6: Distribution of real part of complex permeability in the $h_{lam.} = 2.5$ mm layers of R63 toroid after cutting and sketch for assignment.

Improved attenuation by increasing lamination

The comparison is based on equal effective core parameters (s. table I) for each core size. For the R63 cores, the curves were scaled (sc.) to $A_{eff} = 195.79$ mm². Fig. 8 a) shows the magnitude of the complex impedance of the bulk and the laminated R25 cores at $\vartheta = 25$ °C. The laminated cores have a lower impedance up to about $f = 620$ kHz due to the reduced real part of the permeability. Above this, the impedance increases significantly. The thinner the layers, the more pronounced the improvement. The same can be seen in the measurements at $\vartheta = 100$ °C in fig. 8 b), although the intersection point here is already about $f = 190$ kHz. Compared to the measurements at $\vartheta = 25$ °C the impedances are higher at lower frequencies and lower at higher frequencies. The comparison of the attenuation of the laminated cores with respect to their bulk cores is made according to:

$$A(\mathrm{dB}) = 20 \cdot \log\left(\frac{|\underline{Z}_{lam.}|}{|\underline{Z}_{bulk}|}\right) \tag{5}$$

In fig. 8 c) the attenuation of the laminated R25 cores compared to the bulk cores are depicted at $\vartheta = 25$ °C and in fig. 8 d) for $\vartheta = 100$ °C. Due to the reduced real part of the permeability, the laminated

cores initially show lower attenuation (up to A = -3.0 dB at ϑ = 25 °C and A = -2.4 dB at ϑ = 100 °C). At higher frequencies, the laminated cores show significantly higher attenuation (up to A = 10.7 dB at ϑ = 25 °C and A = 10.4 dB at ϑ = 100 °C). A comparable behavior is also seen in the measurements of the R16 cores in fig. 9 a) and c). For the R63 cores in fig. 9 b) and d), an improvement is obtained due to the increase of the real part of the permeability in the entire curves. The core with $h_{\mathrm{lam.}}$ = 2.5 mm layers shows a reduction of up to A = -0.76 dB in the range of f = 150 - 330 kHz. A maximum attenuation of up to A = 14.7 dB is achieved at f = 3.6 MHz.

CM choke made of laminated T38 toroid

The aim of the work is to substitute a nanocrystalline toroidal core by a laminated T38 ferrite core. The geometry data of the nanocrystalline core are given in table I. For the effective core parameter A_{e} a filling factor (ff) of 70 % is considered. Also, the saturation flux densities of the nanocrystalline core (from measurements) and of the ferrite T38 (from datasheet [1]) are shown in table I. Fig. 7 a) illustrates two of the nanocrystalline cores in housings, b) the nanocrystalline core without the housing and c) a laminated R25 core with 1 mm layers of T38 scaled to the size of the nanocrystalline core.

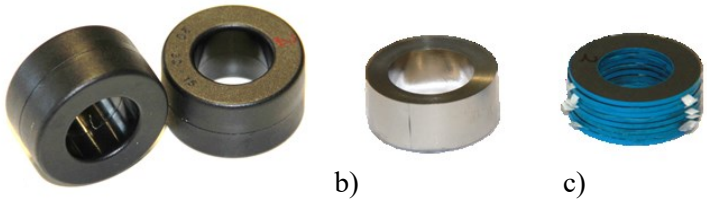

a) b) c)

Fig. 7: a) nanocrystalline cores in housing, b) nanocrystalline core and c) T38 R25 core 8x1mm (sc.).

When designing a CM choke with a small number of turns, the equivalent series circuit of an inductor can be used as a first approximation. The complex impedance follows [3, 4, 14]:

$$\underline{Z} = R(\omega) + \mathrm{j}\omega L \tag{6}$$

Here R represents the occurring losses and L the inductance of the arrangement. The aim is to achieve the highest possible amount of attenuation with the lowest possible material input. In addition, the saturation of the material must be considered [3, 4, 14]:

$$\hat{B} = \frac{L \cdot \hat{I}}{N \cdot A_{\mathrm{e}}} \tag{7}$$

According to the occurring current level $\hat{I}$, it must be ensured that the magnetic flux density $\hat{B}$ is below the saturation flux density $B_{\mathrm{sat.}}$ (s. table I). The ferrite is designed to have the same radii as the nanocrystalline core. The height and the number of turns is adjusted so that the inductance at f = 10 kHz at ϑ = 25 °C is comparable. In addition to the magnitude of the complex impedance, the Q-factor, the quotient of the magnitude of the imaginary part of $\underline{Z}$ to its real part, is a decisive parameter. The smaller the losses, the higher the quality [3, 4, 14]:

$$Q = \frac{|\mathrm{Im}\{\underline{Z}\}|}{\mathrm{Re}\{\underline{Z}\}} = \frac{\omega L}{R} \tag{8}$$

For the complex permeability of the CM chokes made of ferrite, the data of the bulk and those of the R25 core with the thinnest layer thickness $h_{\mathrm{lam.}}$ = 1 mm are used. The material data of the R25 cores were chosen because they are closest to the desired geometry. Since the design is to be carried out up to a frequency of f = 100 MHz, the determined material data must be extrapolated. For this purpose, the modified debye approach described in [18] is used. Fig. 10 a) shows the result for the complex permeability of the nanocrystalline toroid at ϑ = 25 °C. Fig. 10 b) depicts the extrapolated curves of the R25 core made of $h_{\mathrm{lam.}}$ = 1 mm layers. Based on the extrapolated material data, the CM chokes made of nanocrystalline material and T38 ferrite with and without lamination are designed at ϑ = 25 °C and at ϑ = 100 °C according to equations (6-8). For the nanocrystalline choke, one turn (N = 1) is used. To keep the height of the ferrite chokes as low as possible, N = 2 turns are used. Fig. 11 a) shows the magnitude of the complex impedance. The bulk ferrite choke exceeds the impedance of the nanocrystalline choke up to a frequency of f = 8.1 MHz at ϑ = 25 °C and f = 4.7 MHz at 100 °C. After that, it is significantly

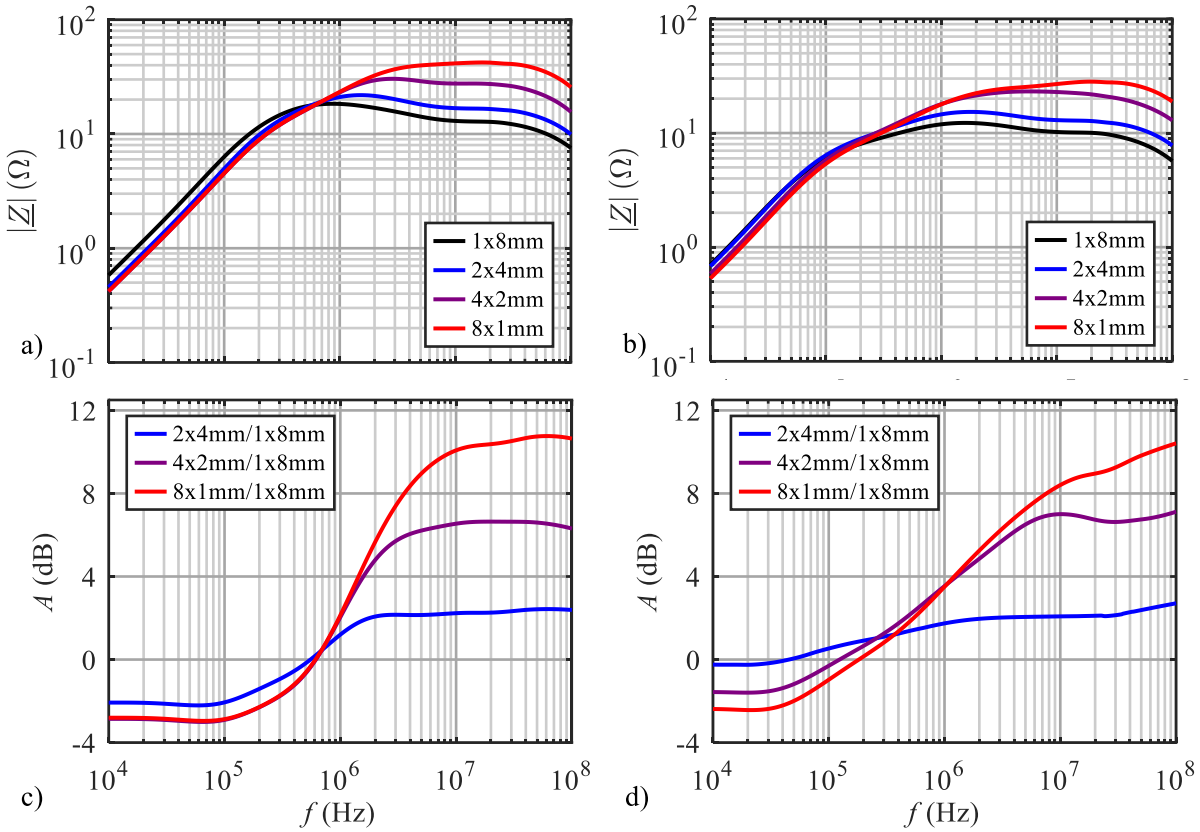

Fig. 8: Magnitude of complex impedance of bulk and laminated R25 T38 cores at a) $\vartheta = 25$ °C, b) $\vartheta = 100$ °C. Attenuation of laminated R25 cores related to bulk cores at c) $\vartheta = 25$ °C, d) $\vartheta = 100$ °C.

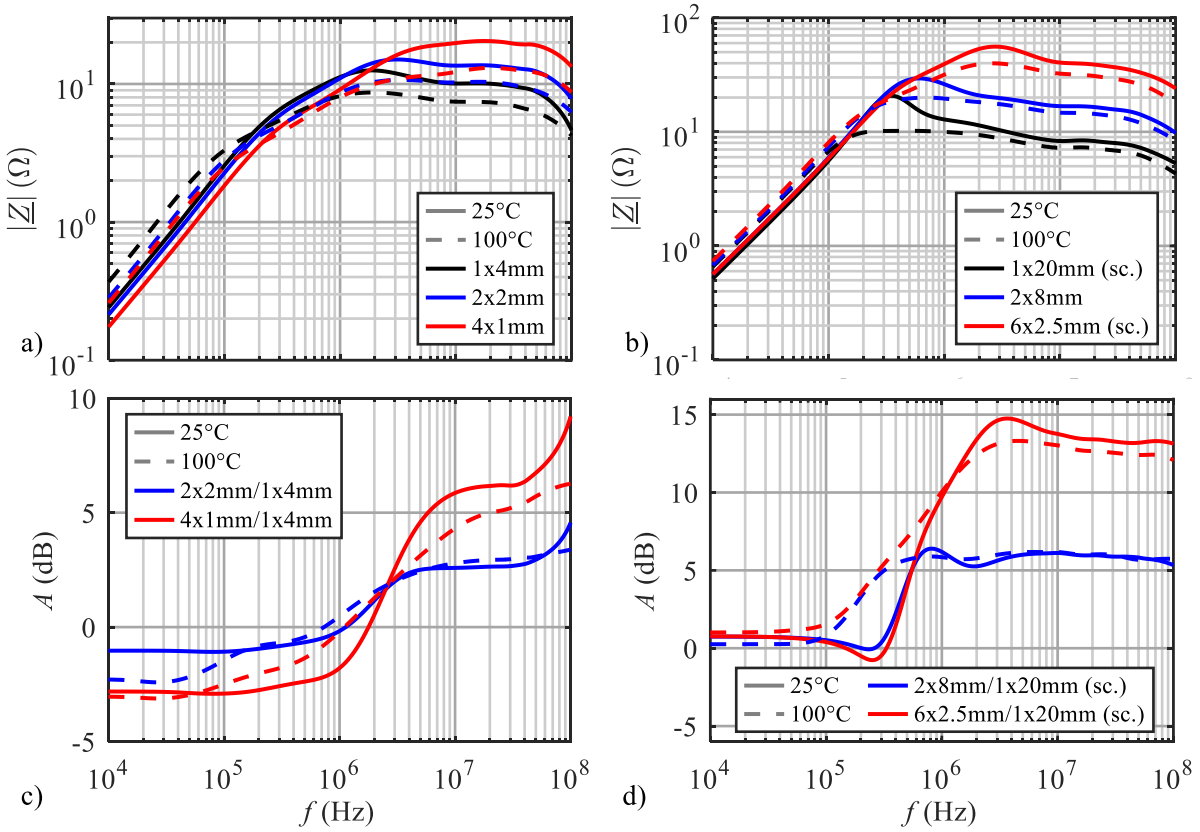

Fig. 9: Magnitude of complex impedance of bulk and laminated T38 cores at $\vartheta = 25$ °C/ 100 °C for a) R16, b) R63. Attenuation of laminated cores related to bulk cores c) R16, d) R63.

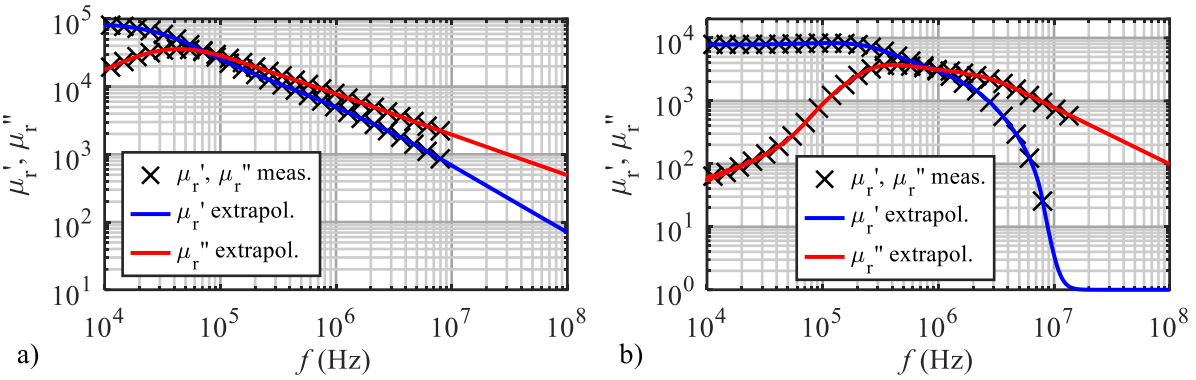

Fig. 10: Extrapolated complex permeability of a) nanocrystalline and b) T38 8x1mm core at $\vartheta = 25$ °C.

lower. The ferrite choke made of laminated layers exceeds the impedance of the nanocrystalline choke in the entire frequency range. For the 100 °C curves, the ferrite chokes are above the curves of $\vartheta = 25$ °C up to $f = 100$ kHz and $f = 170$ kHz. At higher frequencies they are below. The laminated ferrite choke always shows a higher impedance compared to the nanocrystalline core. If we look at the Q-factor shown in fig. 11 b), we see that the ferrite chokes have a higher quality up to the lower MHz range. However, especially at the higher frequencies, the nanocrystalline choke has a higher quality. It should be noted that this is a simplified approach. Resonance effects due to wave propagation are not considered at this point. This can be seen when the curve of the magnitude of the complex impedance of the laminated core is compared to the curves in fig. 8 a) and b). In measurements, the impedance already drops slightly at frequencies above $f = 40$ MHz. When looking at the calculated saturation currents in table II, the disadvantage of ferrite becomes apparent. If the saturation current at $\vartheta = 25$ °C is still above (18.8 % for the bulk and 63.4 % for the laminated ferrite) the nanocrystalline core, it is significantly below (-47.8 % bulk and -31.3 % for the laminated ferrite) at $\vartheta = 100$ °C.

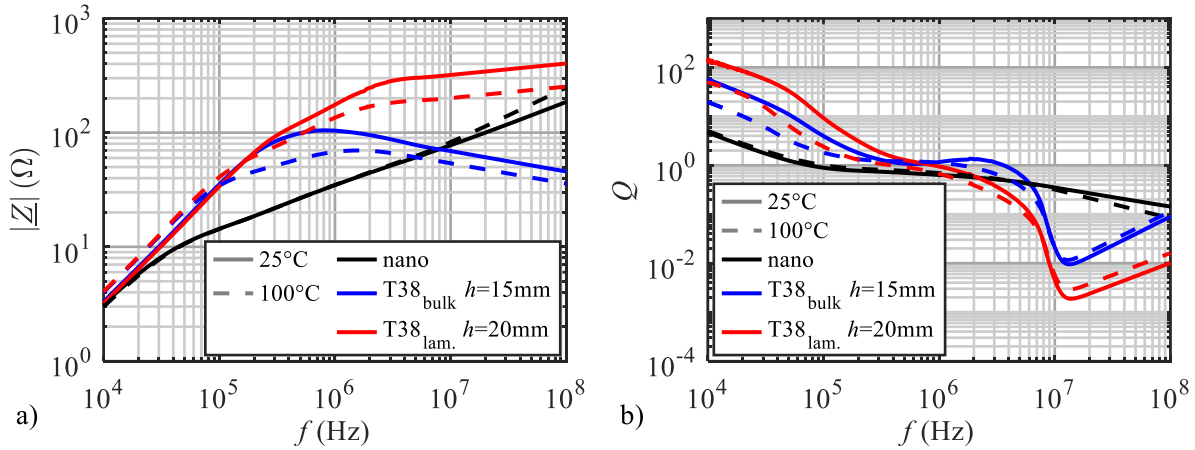

Fig. 11: a) Magnitude of complex impedance of CM chokes made of nanocrystalline material, bulk and laminated T38 ferrite at $\vartheta = 25$ °C/ 100 °C, b) quality factor of the CM chokes.

Conclusion

The substitution of a nanocrystalline core by a laminated ferrite core for a CM choke is possible. Compared to bulk ferrite cores, a significantly improved frequency behavior of the complex permeability and thus of the complex impedance could be achieved. The mechanical machining of the cores influences its magnetic properties. A decrease of the real part of the permeability is detected for smaller cores (R16, R25) in contrast to an increase for the R63 core were measured. It could be shown that for large cores there is a certain distribution of the real part of complex permeability in axial direction which has to be considered for the calculation of the exact distribution of the magnetic flux. The CM choke developed in this work exhibits a higher impedance compared to the nanocrystalline core. However, the Q-factor is worse at higher frequencies. Also, lower saturation currents are achieved at higher temperatures.

Table II: Hight and saturation currents of CM chokes.

core type	h [mm]	$\hat{I}_{\mathrm{sat.,25°C}}$ [A]	$\hat{I}_{\mathrm{sat.,100°C}}$ [A]
nano	15	1.01	1.15
$\mathrm{T38_{bulk}}$	15	1.20	0.60
$\mathrm{T38_{lam.}}$	20	1.65	0.79

References

[1] TDK, "Ferrites and Accessories," EPCOS AG, Munich, 2017, www.epcos.com.

[2] Ferroxcube, "Soft Ferrites and Accessories," Ferroxcube International Holding B.V., Taiwan, 2013, www.ferroxcube.com.

[3] P. Zacharias, "Magnetische Bauelemente," Springer Fachmedien Wiesbaden GmbH, Wiesbaden, 2020, doi: 10.1007/ISBN978-3-658-24742-3.

[4] R. Hilzinger, W. Rodewald, "Magnetic Materials," Publicis Publishing, Erlangen, 2013, ISBN978-3-89578-352-4.

[5] M. Ferch, "Nanocrystalline core materials for modern power electronic designs," Magnetec GmbH, 2003, www.magnetec.de.

[6] M. Kącki, M. S. Ryłko, J. G. Hayes and C. R. Sullivan, "A Study of Flux Distribution and Impedance in Solid and Laminar Ferrite Cores," 2019 IEEE Applied Power Electronics Conference and Exposition (APEC), 2019, pp. 2681-2687, doi: 10.1109/APEC.2019.8722252.

[7] M. Kącki, M.S. Ryłko, J.G Hayes, C.R. Sullivan, E. Herbert, "Magnetic core dimensional effects - flux propagation in ferrites," PSMA Workshop during IEEE Applied Power Electronics Conference, 2018.

[8] J. Zhu, K. J. Tseng, P. Hing and C. F. Foo, "Effects of multi-segment structure in core loss reduction of MnZn ferrite," Proceedings IPEMC 2000. Third International Power Electronics and Motion Control Conference (IEEE Cat. No.00EX435), 2000, pp. 58-63 vol.1, doi: 10.1109/IPEMC.2000.885331.

[9] A. Nagel and R. W. De Doncker, "Systematic design of EMI-filters for power converters," Conference Record of the 2000 IEEE Industry Applications Conference. Thirty-Fifth IAS Annual Meeting and World Conference on Industrial Applications of Electrical Energy (Cat. No.00CH37129), 2000, pp. 2523-2525 vol.4, doi: 10.1109/IAS.2000.883177.

[10] S.-P. Weber, "Effizienter Entwurf von EMV-Filtern für leistungselektronische Geräte unter Anwendung der Methode der partiellen Elemente," Ph.D. dissertation, Faculty IV - Electrical Engineering and Computer Science of the Technical University of Berlin, 2007.

[11] G. R. Skutt, "High-Frequency Dimensional Effects in Ferrite-Core Magnetic Devices," Ph.D. dissertation, Virginia Polytechnic Institute and State University, Blacksburg, VA, 1996.

[12] G.R. Skutt, F.C. Lee, "Characterization of dimensional effects in ferrite-core magnetic devices," Power Electronics Specialist Conference, 1996.

[13] G. Hurley, T. Merkin, M. Duffy, “The performance factor for magnetic materials revisited: The effect of core losses on the selection of core size in transformers,” IEEE Power Electronics Magazine, vol. 5, no. 3, page: 26-34, September 2018.

[14] E. C. Snelling: "Soft Ferrites, Properties and Application," London: Iliffe Books Ltd., 1969, ISBN-13: 978-0592027906.

[15] A. Stadler, M. Albach and A. Bucher, "Calculation of Core Losses in Toroids with Rectangular Cross Section," 2006 12th International Power Electronics and Motion Control Conference, 2006, pp. 828-833, doi: 10.1109/EPEPEMC.2006.4778502.

[16] W. Hauser and M. Albach, "Analytic model of structural effects in toroid cores with rectangular cross section," 2016 6th International Electric Drives Production Conference (EDPC), 2016, pp. 60-66, doi: 10.1109/EDPC.2016.7851315.

[17] A. Stadler, M. Albach and A. Lindner, "A Practical Method to Measure Electrical AC Conductivity of MnZn Ferrites Using Conventional Toroids," in IEEE Transactions on Magnetics, vol. 46, no. 2, pp. 678-681, Feb. 2010, doi: 10.1109/TMAG.2009.2030157.

[18] L. Reissenweber and A. Stadler, "Modeling of a Power Transformer including Higher Order Resonances," 2020 22nd European Conference on Power Electronics and Applications (EPE'20 ECCE Europe), 2020, pp. P.1-P.9, doi: 10.23919/EPE20ECCEEurope43536.2020.9215926.